DOI: 10.13009/EUCASS2022-6105
9TH EUROPEAN CONFERENCE FOR AERONAUTICS AND SPACE SCIENCES (EUCASS)

Low-fidelity Aerodynamic Integration of Distributed Electric Propulsion on a Blended Wing Body including Boundary Layer Ingestion

V.J.E. Aalbers⋆ *and J. van Muijden*⋆†
⋆ *Royal Netherlands Aerospace Centre*
Anthony Fokkerweg 2, 1059CM, Amsterdam, The Netherlands
Jos.Aalbers@nlr.nl · Jaap.van.Muijden@nlr.nl

Abstract

A low-fidelity implementation of Boundary Layer Ingestion (BLI) on ONERA's SMILE Blended Wing Body (BWB) geometry including Distributed Electric Propulsion (DEP)is presented. BLI is modelled using a parallel compressor method taking into account compressibility of the boundary layer. NLR's in-house tool MATRICS-V is used to establish a baseline flow over the geometry. To estimate the performance of the overall system, a Power Balance Method is implemented. The assessed benefit of DEP-BLI is due to a reenergized boundary layer resulting in higher propulsive efficiency. A power savings coefficient shows that propulsive power savings could lead up to 3.1%.

1. Introduction

To meet the demand for a reduced carbon footprint of commercial aircraft, an increasing interest has been taken by the scientific and industrial community to consider disruptive, radical new technologies and configurations.[7,8] One of the options, hybrid-electric propulsion, is currently being investigated within the European project IMOTHEP (Investigation and Maturation Of Technologies for Hybrid-Electric Propulsion) for its merits to reduce fuel consumption. Specifically, a concept that is considered within IMOTHEP is ONERA SMILE Blended Wing Body (BWB), with distributed electric propulsion. In this paper a low-fidelity methodology will be presented how to model Boundary Layer Ingestion (BLI) in conjunction with distributed propulsion, allowing for quick evaluation of a configuration. To model the boundary layer ingestion, a Parallel Compressor Method is employed.[3,9] In this method, the flow is divided in an averaged boundary layer flow and a free flow. The propulsor ingests the boundary layer stream thus reenergizing it.The proposed benefit is a reduced wake loss of the boundary layer. Contrary to classical propulsion without BLI, thrust and drag are now highly coupled. Therefore, to keep track of the thrust and drag terms a Power Balance method is employed.[1,4]

This paper is organized in two parts. The first part will treats the parallel compressor method, its governing equations, including a brief derivation of the boundary layer subsitution model and a parametric study of an isolated propulsor to quantify the potential power savings due to BLI. The parametric study consists of a sweep of different Mach numbers, fan diameters and altitudes. A fixed value of the thrust will be maintained, while the fan pressure ratio will be adjusted accordingly. The second part applies the BLI module to a BWB configuration and assess the performance using the Power Balance Method. A baseline flow is computed using NLR's in-house developed viscous-inviscid interaction full potential flow solver MATRICS-V and these flow results will be complemented with the propulsors including cowling and some of the viscous drag will be ingested by the compressors. The power balance equation is solved using an iterative process based on varying fan diameters or fan pressure ratio.

2. Parallel Compressor Method

The parallel compressor method (PCM) is a typical low-fidelity method to model a propulsor using a 1-dimensional actuator disk theory. In this method, the incoming flow is divided in a 'boundary layer' stream and a 'free flow' stream. In the mathematical formulation which will be presented below, these flows will be subscripted with bl and ff respectively. This will follow to a large extent the description of the model of Plas and Budziszewski.[3,9] A compressor map describes the pressure rise as a function of the incoming mass flow as well as the rate of (thermal) efficiency of

DOI: 10.13009/EUCASS2022-6105

the fan. Before describing the implementation of the PCM, first a boundary layer substitution model will be described to model the boundary layer.

2.1 Boundary layer substitution model

In this section a boundary layer substitution model is described. This model represents the boundary layer by conserving typical boundary layer properties such as the momentum thickness and the boundary layer displacement thickness. To retrieve these boundary layer properties, aerodynamic analysis software such as X-FOIL for two-dimensional and MATRICS-V for three-dimensional flows are used. Both methods are in essence viscous-inviscid interaction solvers Both methods are in essence viscous-inviscid interaction solvers, the former based on boundary integral panel method and the latter based on full potential theory. Typical boundary layer properties at hand with X-FOIL are the shape factor. First a derivation of the boundary layer substitution model based on the shape factor H will be given, followed by a model based on the slightly different formulation, $\overline{H}$. A visual representation of a substitution model is shown in figure 1.

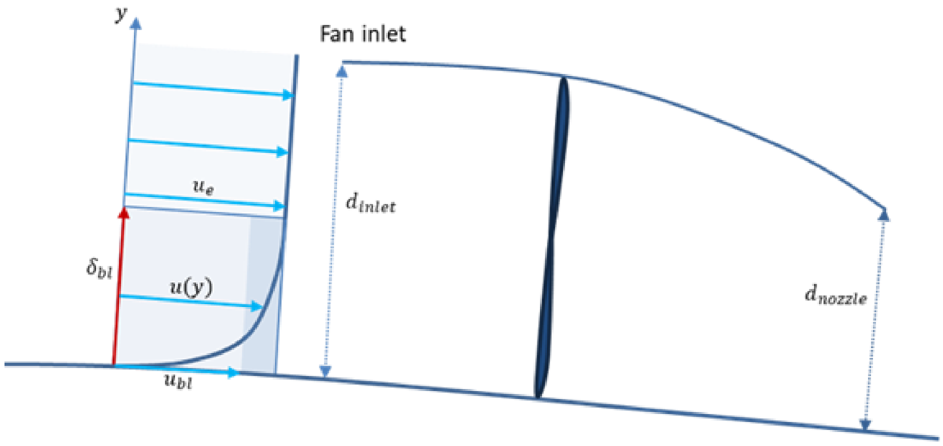

Figure 1: Boundary layer substitution model.

2.1.1 Substitution model based on the shape factor H

The quantities of interest are the shape factor H, the displacement thickness $\delta^\star$ and the momentum thickness θ,

$$H = \frac{\delta^\star}{\theta} \tag{1}$$

$$\theta = \int_0^\delta \frac{\rho u}{\rho_e u_e}\left(1 - \frac{u}{u_e}\right) dy \tag{2}$$

$$\delta^\star = \int_0^\delta \left(1 - \frac{\rho u}{\rho_e u_e}\right) dy \tag{3}$$

where u is the flow velocity in the boundary layer, ρ represents the density of the flow and the edge values denoted with subscript e at height δ from the body. Contrary to PCM method descriptions by Plas and Budziszewski, the boundary layer flow may be compressible in nature. This requires a relation of the flow density throughout the boundary layer. The Crocco relation provides a closed model directly applicable for our cause,[13] the variable r is the recovery factor. Reasonable values are 0.89 for turbulent flows and 0.85 for laminar flows. Note that the flow is assumed to be adiabatic.

$$\frac{\rho_e}{\rho} = \frac{T}{T_e} = 1 + r\frac{\gamma - 1}{2}M_e^2\left(1 - \left(\frac{u}{u_e}\right)^2\right) \tag{4}$$

Later on it may become tedious to write out this relation in its entirety, therefore an identity will be introduced,

DOI: 10.13009/EUCASS2022-6105

$$\frac{\rho_e}{\rho} = \frac{T}{T_e} = 1 + r\frac{\gamma-1}{2}M_e^2\left(1-\left(\frac{u}{u_e}\right)^2\right) \quad := \quad \hat{\alpha} + (1-\hat{\alpha})\frac{u^2}{u_e^2} \tag{5}$$

$$\hat{\alpha} \quad = \quad 1 + r\frac{\gamma-1}{2}M_e^2 \tag{6}$$

The boundary layer substitution model replaces the boundary layer profile by an averaged stream with height δ and constant velocity u_{bl}, while maintaining the local shape factor H. Having two unknowns, this requires two equations. Setting u to u_{bl}, let us now fill in these quantities for the boundary layer displacement thickness $\delta^\star$,

$$\delta^\star = \int_0^\delta \left(1 - \frac{\rho u}{\rho_e u_e}\right) dy \rightarrow \delta^\star u_e = \int_0^\delta \left(u_e - \frac{\rho}{\rho_e}u\right) dy \rightarrow \delta^\star u_e = \left(u_e - \frac{\rho_{bl}}{\rho_e}u_{bl}\right)\delta_{bl}. \tag{7}$$

The same can be applied to the boundary layer momentum thickness θ,

$$\theta = \int_0^\delta \frac{\rho u}{\rho_e u_e}\left(1 - \frac{u}{u_e}\right) dy \rightarrow \theta u_e^2 = \int_0^\delta \frac{\rho}{\rho_e} u\,(u_e - u)\,dy \rightarrow \theta u_e^2 = \frac{\rho_{bl}}{\rho_e} u_{bl}\,(u_e - u_{bl})\,\delta_{bl}. \tag{8}$$

Filling in the identity for the Crocco relation, we end up with,

$$\theta u_e^2 \quad = \quad u_{bl}\,(u_e - u_{bl})\left(\hat{\alpha} + (1-\hat{\alpha})\frac{u_{bl}^2}{u_e^2}\right)^{-1}\delta_{bl} \tag{9}$$

$$\delta^\star u_e \quad = \quad \left(u_e - \left(\hat{\alpha} + (1-\hat{\alpha})\frac{u_{bl}^2}{u_e^2}\right)^{-1} u_{bl}\right)\delta_{bl}. \tag{10}$$

Solving for the boundary layer velocity, u_{bl} and rearranging the terms yields the following equation,

$$u_{bl} = \frac{u_e\,(H+1) \pm u_e\,((H+1) - 2\hat{\alpha})}{2\,(H+1) - 2\hat{\alpha}}. \tag{11}$$

From the last equation it can readily be seen that addition of the solution yields a trivial solution, $u_{bl} = u_e$. This is not a very useful result for our boundary layer substitution model. The other solution becomes,

$$u_{bl} = \frac{\hat{\alpha}}{(H+1) - \hat{\alpha}}u_e \tag{12}$$

This concludes the boundary layer substitution model for a boundary layer based on the regular shape factor H, which can be used for applications with for instance, X-FOILwhere this information can be found directly. Note that for incompressible flow, the Mach number is 0, ($M_e = 0$), reducing $\hat{\alpha}$ to 1 resulting in $u_{bl} = u_e/H$, which is a result found in.[3,9] In the following section, a derivation will be done based on a slightly different formulation, $\overline{H}$. This formulation is used in MATRICS-V.

2.1.2 Subsitution model based on the shape factor $\overline{H}$

As stated before, the metrics describing the boundary layer in MATRICS-V is slightly different than X-FOIL. Instead of using the shape factor H, a slightly different formulation using an equivalent incompressible shape factor denoted with $\overline{H}$ is applied, and is defined as,

$$\overline{H} = \frac{1}{\theta}\int_0^\infty \frac{\rho}{\rho_e}\left(1 - \frac{u}{u_e}\right) dy \tag{13}$$

where θ is the momentum thickness as described in equation 2. Using this definition, the same steps can be taken as described in section 2.1.1 to find out that,

$$u_{bl} \quad = \quad \frac{u_e}{\overline{H}} \tag{14}$$

$$\delta_{bl} \quad = \quad \frac{\theta\left(\hat{\alpha}\overline{H}^2 + 1 - \hat{\alpha}\right)}{\overline{H} - 1} \tag{15}$$

DOI: 10.13009/EUCASS2022-6105

To see why this is equivalent to the boundary layer substitution model in the section 2.1.1, use the identity that relates the shape factor H to $\overline{H}$:

$$(H + 1) = \left(\overline{H} + 1\right)\left(1 + \frac{\gamma - 1}{2} M_e^2\right) = \left(\overline{H} + 1\right)\hat{\alpha} \tag{16}$$

2.2 Implementation of PCM

In the low fidelity approach using Parallel Compressor Method, two distinct streams are going through the propulsor. These streams do not interact with one another, although at some stages throughout the flow it is assumed that the local static pressure is uniform across both streams. A diagram with the control volume is shown in figure 2a.

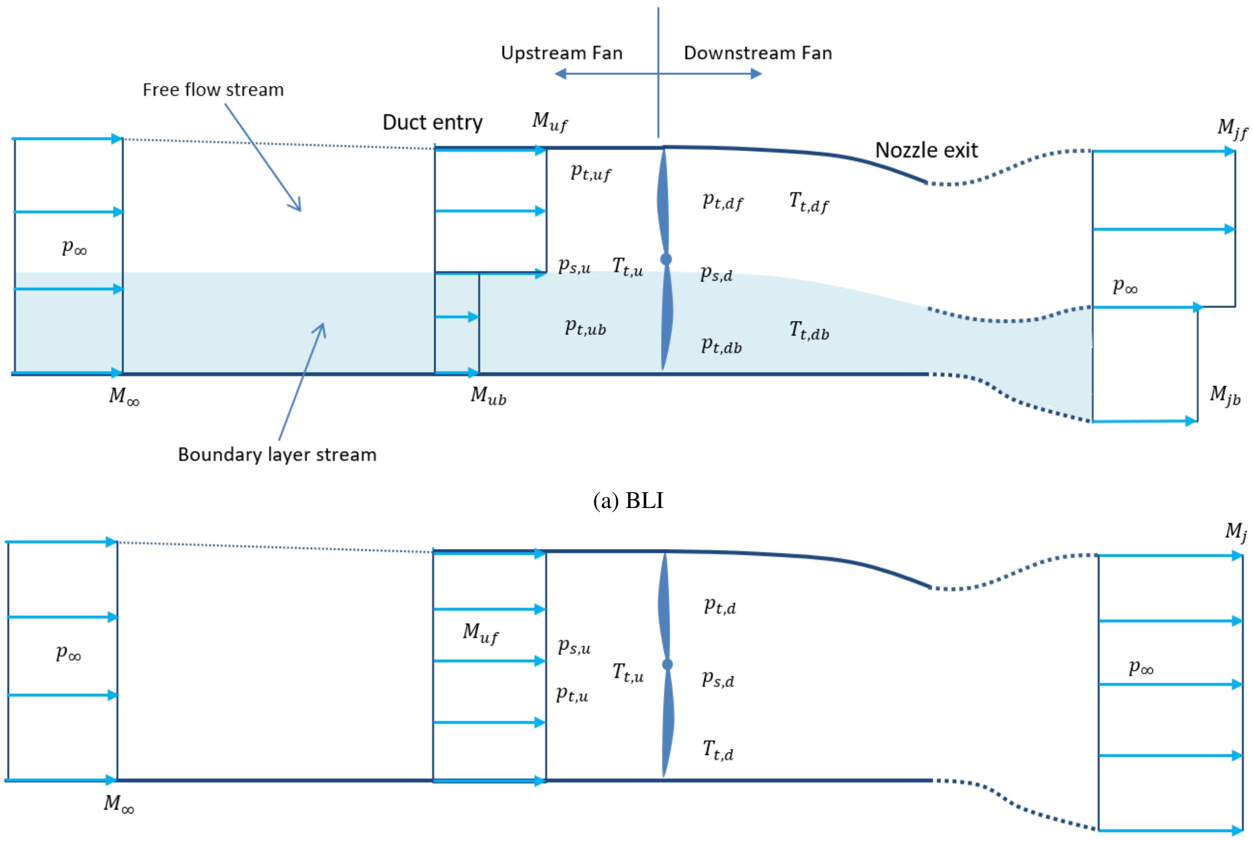

Figure 2: Control volume of the flow through the propulsor with (top) and without (bottom) BLI.

Throughout this section, the edge stream (or free flow) is denoted with subscript ff, while the boundary layer stream is denoted with the subscript bl. A placeholder subscript k is reserved for a generic notation, free flow or boundary layer stream. The free flow stream is assumed to be isentropic outside the propulsor. Inside the propulsor, the total temperature, T_t and total pressure, p_t, are increased by the propulsor by a certain amount. A compressor map describes these temperature and pressure rises, τ and Π, respectively , as a function of the (corrected) massflow,

$$\Pi_k = \frac{p_{t,dk}}{p_{t,uk}} = f(\dot{m}_k) \tag{17}$$

$$\tau_k = \frac{T_{t,dk}}{T_{t,u}} = g(\dot{m}_k). \tag{18}$$

Although the free flow pressure and temperature rise are given, it is assumed that the compressor map is applicable to the boundary layer stream as well. In this low-fidelity approach, the compressor map is treated as input. The total temperature rise is also dependent on the isentropic efficiency, η_{KE}, which is also part of a compressor map. This effiency could be isentropic efficiency, described by Plas[9] or a polytropic efficiency as formulated by Sgueglia.[11]

DOI: 10.13009/EUCASS2022-6105

As the boundary layer is assumed to be adiabatic, the total temperature at the fan inlet inlet is homogeneous over both streams. From this the static temperature, and boundary layer Mach number $M_{u,b}$ can be computed,[10]

$$\begin{aligned} M &= \frac{u}{a} & \frac{p_t}{p} &= \left(1 + \frac{\gamma-1}{2}M^2\right)^{\frac{\gamma}{\gamma-1}} \\ a &= \sqrt{\gamma R T} & \frac{T_t}{T} &= \left(1 + \frac{\gamma-1}{2}M^2\right). \end{aligned} \tag{19}$$

After passing the fan, the total pressure and temperature will be different as the mass flow of each stream is different. The mass flow for compressible flows is computed as follows,

$$\dot{m}_k = \frac{A_k p_{t,k}}{\sqrt{T_{t,k}}} \sqrt{\frac{\gamma}{R}} M_k \cdot \left(1 + \frac{\gamma-1}{2}M_k^2\right)^{-\frac{\gamma+1}{2(\gamma-1)}}, \tag{20}$$

where A is the inlet area of the free flow and boundary layer streams. Knowing the boundary layer height δ, and the fan diameter, some simple geometric relations can be applied to find the area of the boundary layer and the free flow, respectively.

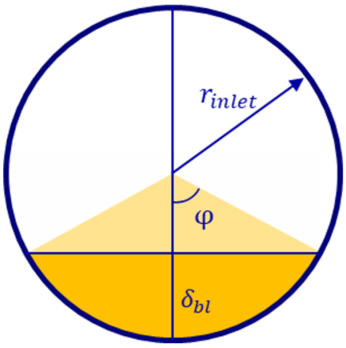

Figure 3: Schematic of the affected area by the boundary layer.

From figure 3, the area of the boundary layer at the bottom of the inlet, it can be derived that,

$$A_{total} = \pi r_{inlet}^2 \tag{21}$$

$$\varphi = \arccos\left(1 - \frac{\delta}{r_{inlet}}\right) \tag{22}$$

$$A_{bl} = \varphi \cdot r_{inlet}^2 - r_{inlet} \cdot \sin(\varphi) \cdot (r_{inlet} - \delta), \tag{23}$$

where it is assumed that the flow is never chocked. When all the relevant quantities such as jet velocities, $u_{j,k}$ and massflows $\dot{m}_k$ are known for both streams, the thrust, propulsive power and shaft power can be determined,

$$T = \sum_k \dot{m}_k \left(u_{j,k} - u_\infty\right) \tag{24}$$

$$P_P = \sum_k \frac{\dot{m}_k}{2} \left(u_{j,k}^2 - u_\infty^2\right) \tag{25}$$

$$P_S = \sum_k \dot{m}_k \cdot c_p \left(T_{t,k} - T_{t,\infty}\right) \tag{26}$$

where the summation over k depicts to sum over both the boundary layer stream as well as the free flow stream and c_p is the specific heat at constant pressure.

3. Power Balance Method

Several ways of looking at the power balance and energy paths in aerodynamic flows have been established, useful for different levels of analysis at different moments in the design phase. The application possibilities of these methods

DOI: 10.13009/EUCASS2022-6105

depend on the progress made in the design process and the availability of detailed (geometrical) data. The most complete and comprehensive approach including the thermal part of the balance seems to be the exergy analysis of Arntz,[1] while the slightly older approach of Drela[4] focuses on the flight physics part of the equation. For the currently intended low-fidelity analysis, we will focus on a specific application of Drela's method. Following Drela[4] by investigating the power balance method averaged over a periodic-unsteady interval for a certain control volume, the following power balance is obtained between inflow, outflow and dissipation of power:

$$P_S + P_V + P_K = \dot{\varepsilon} + \Phi \tag{27}$$

Here, on the left hand side, we see respectively the shaft power P_S entered into the fluid from moving surfaces (propellers, fans), the volumetric mechanical power P_V exhibited by the fluid expanding against atmospheric pressure, and the mechanical energy inflow rate P_K into the control volume. On the right hand side we see the mechanical energy flow rate ($\dot{\varepsilon}$) out of the control volume and the viscous dissipation rate Φ. For practical calculations, we will elaborate on these five terms to get a physical meaning and relevance. For cases without moving surfaces (glider-like configuration without propulsion), there will be no power deposited in the flow and P_S can be set equal to zero. Such cases will be compared with traditional drag bookkeeping methods to identify the meaning of the various terms in the power balance as compared to those classical drag terms. The volumetric mechanical power P_V is usually ignored. It will have a strong net contribution at locations where heat is added at a pressure far from ambient (e.g. when a combustor is embedded in the control volume or when external combustion is present like an afterburner), or in supersonic flow where the shock wave system interferes with the Trefftz plane. For glider types of aircraft, we can safely ignore this term, whereas for the supersonic flow a rationale for this approach is obtained by letting the control volume expand to infinity such that any shock waves leave the flow through the sides of the domain before reaching the Trefftz plane. The mechanical energy inflow rate P_K is simply the kinetic energy per second due to free stream flow entering the control volume. On the right hand side, the term $\dot{\varepsilon}$ denotes the mechanical energy flow rate out of the control volume. This term needs some further interpretation to understand its meaning. First of all, it can be written as

$$\dot{\varepsilon} = W\dot{h} + \dot{E}_A + \dot{E}_V + \dot{E}_P + \dot{E}_W. \tag{28}$$

Here, the first term on the right hand side denotes the potential energy rate, which can be rewritten as

$$W\dot{h} = -F_X = Wu_\infty \sin\gamma, \tag{29}$$

where the $x-$ axis is now chosen along the flight path. This is the power consumption needed to increase the aircraft's potential energy, and becomes a source of power during descend. The other term on the right hand side consist of the term $\dot{E}_A$ which is the wake stream wise kinetic energy deposition rate, the term $\dot{E}_V$ that denotes the wake transverse kinetic energy deposition rate, the term $\dot{E}_P$ that denotes the wake pressure-defect work rate, and the term $\dot{E}_W$ which is the wave pressure-work and kinetic energy outflow rate.

Upon comparison of the power balance method with classical momentum conservation theories (force-based analyses), the interpretation of the terms outside of viscous wakes and propulsion plumes becomes

$$\dot{E}_A + \dot{E}_V + \dot{E}_P = D_i u_\infty, \tag{30}$$

i.e. the induced drag times the flight speed. Similarly, the term $\dot{E}_W$ can be interpreted as the wave drag power term,

$$\dot{E}_w = D_w u_\infty \tag{31}$$

So, in a low-fidelity approach we could say that

$$\dot{\varepsilon} = WV_\infty \sin\gamma + D_i u_\infty + D_w u_\infty \tag{32}$$

The advantage to do it in this way lies in the reliable prediction of induced and wave drag components from classical wing and wing-fuselage analysis methods based on strong viscous-inviscid interaction using for example full-potential theory and integral boundary layers, which could then provide the baseline power balance in a very straightforward manner. The last term in the original equation is the term Φ, which denotes the dissipation. If the dissipation is calculated in the case the Trefftz-plane is still assumed closeby, then the following assumptions hold in the jet behind an isolated propulsor:

$$\Phi_{jet} = P_S\,(1 - \eta_{overall}) \tag{33}$$

The overall efficiency can be computed as follows,

DOI: 10.13009/EUCASS2022-6105

$$\eta_{isen} = \frac{P_P}{P_S} \tag{34}$$

$$\eta_p = \frac{T \cdot u_\infty}{P_P} \tag{35}$$

$$\eta_{overall} = \eta_{isen} \cdot \eta_p = \frac{T \cdot u_\infty}{P_S} \tag{36}$$

where, in the case of BLI, the summation over both streams to compute the thrust and power are implied. All in all, a power balance equation can now be build with the aforementioned terms. The equation to solve will become as follows,

$$P_S = D_i \cdot u_\infty + D_w \cdot u_\infty + D_V \cdot u_\infty + \Phi_{jet} + P_{excs} \tag{37}$$

where P_{excs} is denoted as excess power which can be used to gain potential energy (i.e. climb), and is defined as equation 29.

3.1 Adding propulsor components to the Baseline Flow

The intention is to use the NLR-developed flow solver MATRICS-V,[12–14] based on strong viscous-inviscid interaction of a full-potential description of the inviscid outer flow and an integral boundary layer method of the viscous shear layer and wake. It should be noted that the boundary layer data from MATRICS-V consist of momentum thickness θ, equivalent incompressible shape factor $\overline{H}$, cross flow parameter C, and boundary layer edge velocity, u_e. The advantage of this flow solver is that it provides an automatic, quick, well-validated drag balance based on classical momentum theory. The components of drag (induced, wave, and viscous drag coefficients) are separately identified which is almost naturally done in such a zonal interaction method. These components are then readily applied to fill the induced, wave and viscous power terms in the power balance method for the baseline configuration. Thus, we can provide the following drag terms in the power balance with confidence for the wing or wing-body configuration (we succeeded to mesh the blended wing-body configurations representative for the SMR-RAD as a stand-alone wing)

$$\begin{aligned} D_i &= C_{D_i}\frac{1}{2}\rho_\infty u_\infty^2 S, \\ D_w &= C_{D_w}\frac{1}{2}\rho_\infty u_\infty^2 S, \\ D_V &= C_{D_V}\frac{1}{2}\rho_\infty u_\infty^2 S, . \end{aligned}$$

The disadvantage of this flow solver is that it is a dedicated flow solver for either stand-alone wing or wing-body configurations. So, there is no possibility to include the propulsion system in the computation of the flow when using this particular flow solver. In the next section a schematic implementation of the Power balance method in conjunction with BLI using a baseline flow will be discussed.

3.2 Implementation of PBM

In this section a practical approach is used for the current low-fidelity analyses. This consists of an iterative approach to solve the power balance equation, equation 37. It is iterative in nature, as the viscous drag is dependent on the inlet area (wetted area of the cowling for the fans), which affects the massflow, and thus the power and thrust. Alternatively, the pressure ratio could be treated as a variable keeping the inlet area constant in order to solve equation 37. The steps to be taken are as follows. A flow chart is shown in figure 4.

1. Compute the baseline (i.e. the non-propelled) configuration using the MATRICS-V flow solver to obtain the three drag coefficients for induced, wave and viscous drag.

2. Use the drag coefficients to calculate the power balance terms for the baseline configuration. The total drag is equal to the propulsive power, P_{prop}.

3. Use the baseline boundary layer data as obtained from the MATRICS-V flow solver to estimate the ingestion aspects, and inlet conditions at the assumed locations of the propulsors, using the parallel compressor method as

DOI: 10.13009/EUCASS2022-6105

implemented in the analysis tool. The definition of ingested drag is the same as the definition used by Plas et. al.,[9]

$$D^{i}_{ingested} = \rho_0 u_\infty^2 \theta_0 d \left(\frac{u_0}{u_\infty}\right)^{H_{avg}} \tag{38}$$

where the density, ρ, inlet velocity u_0, the boundary layer momentum thickness θ_0 and d are all quantities at the inlet of the proplulsor and H_{avg} is the average shape factor of the inlet of the propulsor and the shape factor in the wake. $C^{ingested}_{d_v}$ is the ingested drag coefficient divided by $0.5 \cdot \rho_\infty \cdot u_\infty^2$.

4. Subtract the ingested part of the boundary layer from the baseline data.

$$C'_{d_V} = C_{d_V} - C^{ingested}_{d_V} \tag{39}$$

5. Add the propulsor jet dissipation part to the baseline data.

$$\Phi_{jet} = P_s\left(1 - \eta_{overall}\right) \tag{40}$$

6. Estimate the propulsor cowling dissipation part and add this to the baseline data.

$$C^{cowling}_{d_V} = \sum_i f\left(d_i\right) \tag{41}$$

A flat plate analogy is used to estimate the cowling drag contribution. A MATLAB® routine *friction*[6] is incorporated in the tool which estimates the drag of the cowling using a Karman-Shoenherr formula for turbulent flows,

$$C_F = 2 \cdot \frac{0.242}{\sqrt{C_F}} \log\left(RE_X \cdot C_F\right) \tag{42}$$

while the nacelle is regarded as a blunt body. A form factor FF is used to account for its blunt shape,

$$FF = 1.0 + 1.5\left(\frac{d}{l}\right)^{1.5} + 50\left(\frac{d}{l}\right)^{3} \tag{43}$$

7. Update the Power balance equation with the updated terms,

$$\Phi = \Phi_{jet} + q_\infty C_{d_V} u_\infty \tag{44}$$
$$P_s^{j+1} = \dot{\varepsilon} + \Phi \tag{45}$$

8. Compare the previous value of the shaft power with the new shaft power, if changes with magnitude smaller than μ detected, quit iteration, otherwise go to step 3 to change the fan pressure ratio or the fan diameter. The value for μ is chosen to be 1×10^{-6}.

3.3 BLI vs. NO BLI

The power savings coefficient is often cited to quantify the benefits of BLI. It compares the amount of power a configuration uses without BLI to the situation where BLI is enabled. For this it is required to specify how these comparisons are made, and what a 'NO BLI' configuration constitutes in this case. The definition of the power savings coefficient (PSC), is as follows,

$$PSC = \frac{P_{NO\ BLI} - P_{BLI}}{P_{BLI}} \tag{46}$$

The power could be a shaft power, or propulsive power. By regarding the shaft power, the thermodynamic efficiency of the fan is taken into account, while comparing the PSC with propulsive power the aero-mechanical aspects are considered. The comparison made between BLI and NO BLI is graphically shown in figure 2. Figure 2a shows the BLI setting while on the bottom figure 2b shows the NO BLI setting. Notice that the inlet Mach numbers are for each the same thus having a similar inflow condition. Naturally, the NO BLI setting has no boundary layer. The control volume in both cases ends in the far field where the flow has isentropically has expanded to atmospheric pressure conditions, p_∞.

DOI: 10.13009/EUCASS2022-6105

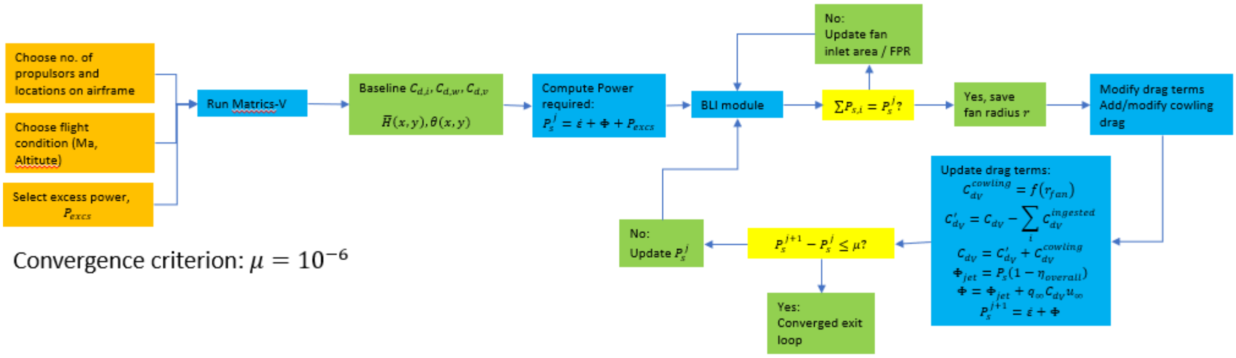

Figure 4: Flow chart to solve the Power Balance Equation (equation 37).

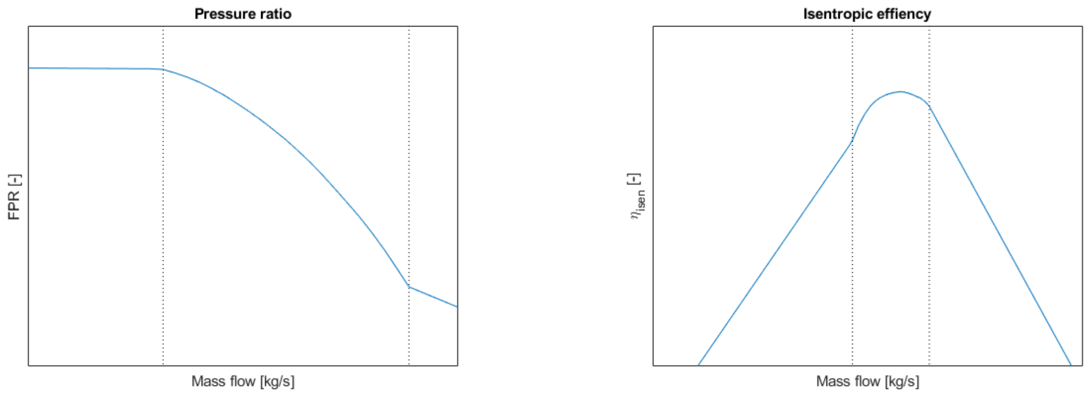

(a) Fan pressure ratio curve.

(b) Efficiency curve.

Figure 5: Example of a compressor map

3.4 The compressor map

A compressor map is used to determine the fan pressure ratio and its corresponding isentropic efficiency as a function of the incoming massflow. It constitutes a set of curves for each motor setting (i.e. RPM setting). This map is usually obtained with high fidelity CFD analyses, but for this low fidelity tool this map for a specific propulsor is an input. An example of such a compressor map is depicted in figure 5. The pressure ratio used in this paper is in the order of 1.15. The black dotted lines constitutes an area where the compressor map is defined, outside this region an assumed behaviour (i.e. extrapolation) is defined. For BLI this compressor map provides the FPR and efficiency for both the free stream as well as for the boundary layer stream. As the massflow of the boundary layer stream usually is quite low, (the boundary layer being a thin layer of air, which also is slowed down significantly due to viscosity), hence extrapolation of the compressor map is required. The overall isentropic efficiency of the fan is determined by massflow averaging the efficiencies of the free stream and the boundary layer stream.

4. Application of DEP-BLI

In this chapter some results are presented using the methods described earlier. The model to be used is ONERA's BWB Smile configuration. This model will be briefly described first followed by some results in the typical cruise section flight conditions which are taken from the Top Level Aircraft Requirements (TLARS).[5]

4.1 Blended Wing Body: SMILE

The SMILE configuration is a blended wing body, designed for small to medium range TLAR's are:

- 150 pax @ 90kg

DOI: 10.13009/EUCASS2022-6105

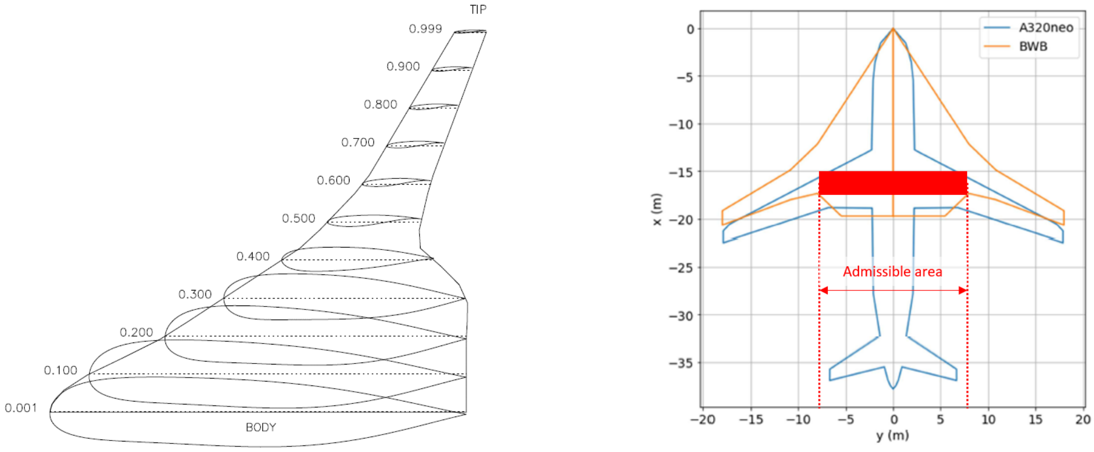

(a) Stack of profiles that constitutes the BWB-SMILE.

(b) Admissible propulsor area.

Figure 6: BWB-Smile configuration[5]

.

- Range: $5100km$
- Cruise Mach number: 0.78 (at an altitude of $12.6km$)

There are two CFM LEAP-1A turbofan engines delivering the electric power for all the systems including the electric fans propelling the aircraft. The turbofans do not deliver any thrust. The reference area is $268.602m^2$, while the reference length is the span width of $36m$. A C_L coefficient of 0.10 and 0.25 are selected to see the effect of different weight cases during cruise and will be referred to as the 'low' and 'high' weight case, respectively. The scheme of the stacked profiles that constitutes the BWB is shown in figure 6a. Notice that in MATRICS-V the winglets have been omitted simplifying the geometry. The middle section of the BWB has a straight 'boxed like' trailing edge making it a suitable area to place propulsors. It is assumed that the admissible area, the red box as sketched in figure 6b is located at 17 meters aft of the BWB nose, and spans 8 meters total. Configurations requiring propulsors beyond this box (e.g. such large fan diameters that part of the mid-wing has to be used for propulsor placement) are deemed unacceptable. Finally, the presence of S-ducted fans have been omitted as the fan duct analysis requires detailed CFD analysis which is beyond the scope of this tool. Instead, a correction at the fan inlet is done that accounts for this S-duct. The computed inlet Mach number M_{uf} (see also figure 2) done by MATRICS-V is replaced by a M_{uf} obtained from high fidelity analysis performed by ONERA[2]

4.2 Effects of distributed propulsion

A benefit of distributed propulsion is that the power is delivered by an array of smaller thrusters. A larger number of thrusters would mean that the power delivered per thruster would be smaller, thus requiring a smaller fan radius for a given fan pressure ratio. Consequently, the relative contribution of the boundary layer would increase hence potentially harnessing positive BLI effects. First, a the number of thrusters will be evaluated as well as the effect of the weight of the aircraft.

4.2.1 Number of thrusters

In the following analysis there will be 6, 8, and 10 thrusters evaluated. The PSC for each configuration as a function of the fan diameter is shown in figure 7 for these configurations. From this figure it can be seen that the actual power savings coefficient could be up to 3.4% for the 10 propulsor low weight case. Also, the BLI returns are diminishing with higher fan diameter as the relative contribution of the boundary layer decreases. It is for both C_L cases clear that a higher number of thrusters leads to larger power savings coefficient. However, the PSC for the high weight case is about 1% smaller than for the low weight case, because the absolute power savings is about the same while the total propulsive power for $C_L = 0.25$ is about $2MW$ higher than for the $C_L = 0.10$ weight case, as a larger weight requires a larger angle of attack resulting in significantly more drag. The angle of attack for the low weight case is 1.11° while for the heigh weight case is about 3.10°. Continuing this paper, for brevity only the weight case $C_L = 0.10$ results will be shown.

DOI: 10.13009/EUCASS2022-6105

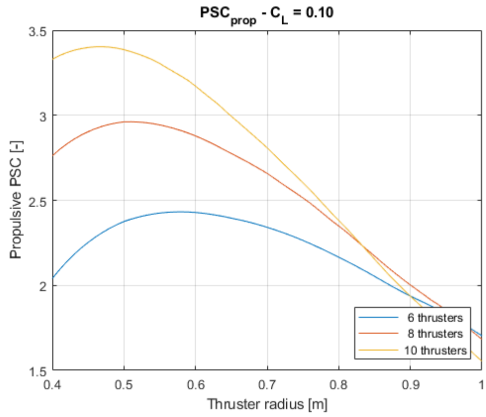

(a) Propulsive Power Savings Coefficient for $C_L = 0.1$.

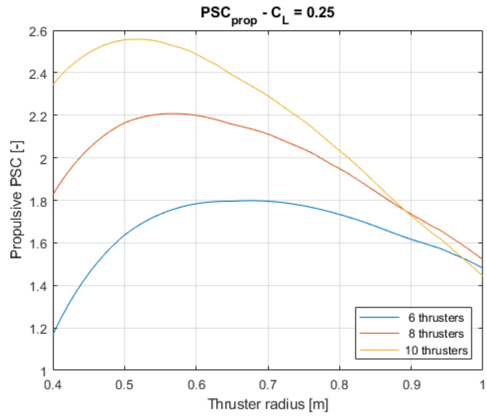

(b) Propulsive Power Savings Coefficient for $C_L = 0.25$.

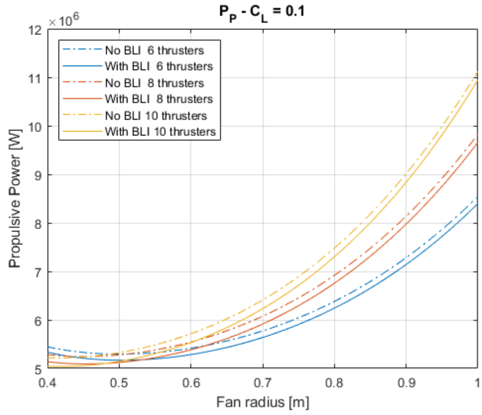

(c) Propulsive Power for $C_L = 0.1$.

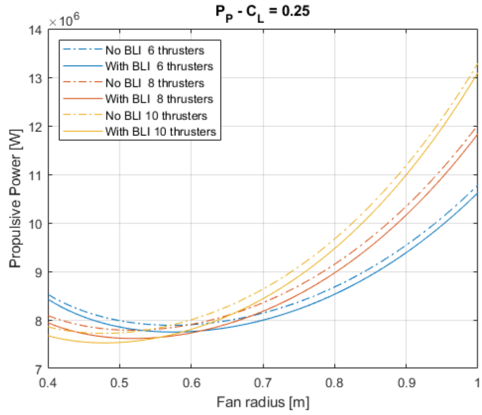

(d) Propulsive Power for $C_L = 0.25$.

Figure 7: BWB-Smile configuration.

All in all, from figure 7 it can be observed that the 'optimum' diameter for 6, 8 and 10 thrusters in terms of PSC and absolute propulsive lies in the same region. The highest PSC (figure 7a) corresponds with a fan diameter which requires the least amount of propulsive power (figure 7a). For the $C_L = 0.1$ case, the minimum propulsive power is 5.1691, 5.0923 and 5.0402 MW for 6, 8 and 10 propulsors respectively, showing a diminishing return with increasing propulsors. A similar analysis can be made with the PSC, even though the fan diameter decreases (and thus the drag decreases) with increasing number of propulsors. As stated before, the DEP configuration is bound to geometrical constrains as the propulsors needs to physically fit on the 'square like' middle section at the trailing edge of the BWB. Configurations that extend beyond 8 meters in span are unsuitable. Figure 8 shows the results of the propulsors for one side of the configuration with and without BLI. Attentive readers could notice that this configuration has a very poor isentropic efficiency which is about 27% which will be discussed later. The location of the outermost propulsor is located at $4.53m$, which is too far outboard to fit on the aircraft and hence will be disregarded for future analysis. Henceforth, only the configuration with 8 thrusters will be taken into account.

4.2.2 Shaft power requirement

Although propulsive power is a measure how much power is required to overcome the dissipative terms such as drag and jet dissipation, a more suitable measure of the power to be delivered by the power train is the shaft power. Recalling equation 35 the relation between the propulsive power and shaft power goes through the isentropic efficiency which, in turn, is part of the compressor map. The shaft power is plotted for various fan diameters as well in figure 9. It can be seen that the required shaft power varies strongly over the range of fan diameters. It is also for this reason that the isentropic efficiency in figure 8 is so low. Figure 8 also shows that the minimum shaft power lies at around $0.9m$ fan radius. An explanation could be that the isentropic efficiency with BLI is compromised due to the boundary layer stream, resulting a higher shaft power at smaller fan radius domain. As the fan radius increases, the relative contribution of the boundary layer on the total mass flow decreases. All in all, comparing figure 7c with figure 8 an optimum fan radius is dependent on the metric to be considered (i.e. minimum propulsive power $r_{fan} \approx 0.5m$ versus

DOI: 10.13009/EUCASS2022-6105

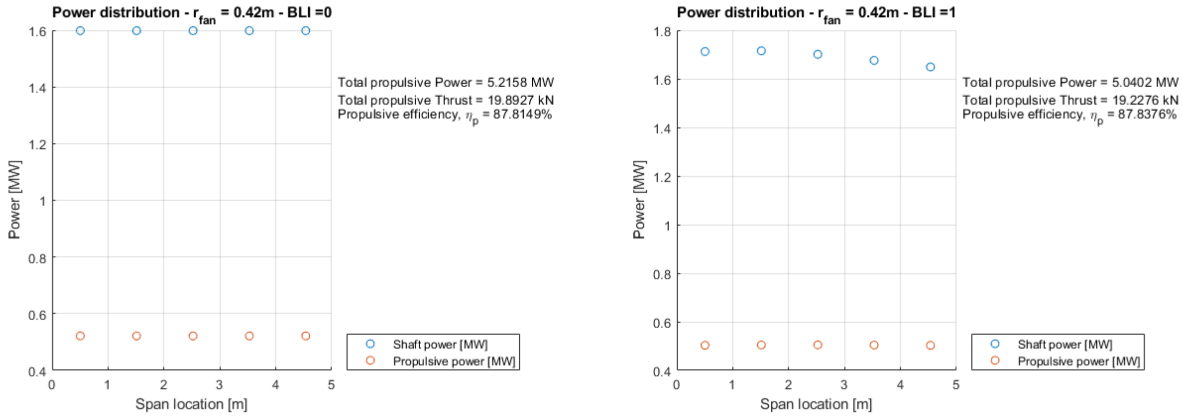

(a) DEP performance - 10 thrusters (BLI is off) (b) DEP performance - 10 thrusters (BLI is on)

Figure 8: DEP performance comparison between BLI off and BLI on.

minimum shaft power at $r_{fan} \approx 0.9m$).

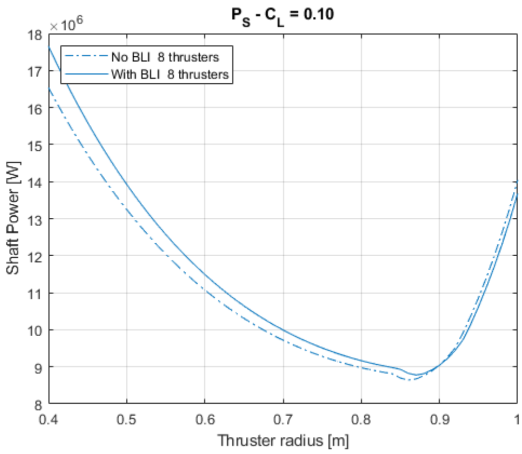

Figure 9: Required shaft power as a function of the fan diameter. BLI vs. No BLI.

Figure 10 shows the overall performance of the array of thrusters. Comparing BLI on with BLI off, it can be seen that the power distribution with BLI off is roughly evenly distributed over the propulsors, while with BLI on this is not the case. This is due to the varying boundary layer properties over the wing and its effect on the power generation per propulsor. Regarding the BLI on case, it can be seen that the inner propulsors require higher shaft power than the outer thrusters, while the propulsive power is about the same. Notice also that the ingested drag (which is equal to the total propulsive thrust) is modest, the thrust difference between BLI on and BLI off is about $650N$ which is on the total of $31kN$ about 2% thrust reduction.

5. Concluding remarks

In this paper a low fidelity methodology is presented to model Distributed Electric Propulsion in conjunction with Boundary Layer Ingestion. The method is based on the Parallel Compressor method which treats the free undisturbed incoming flow and the boundary layer flow separately. For the boundary layer flow, a boundary layer substitution model is presented based conserving basic boundary layer properties such as the shape factor, H, and the boundary layer thickness, $\delta^\star$ and the boundary layer momentum thickness θ. Contrary to what has been published in literature, the presented boundary layer substitution model does account for compressibility of the flow using the Crocco relations.

As this concerns a low fidelity approach, the use of assumptions is inevitable. The boundary layer substitution model is a significant simplification of a very complex turbulent flow. In this approach, there is no interaction between the computed baseline flow and the fan (ducts), is the effect of the accelerated boundary layer on the induced lift (and drag) neglected and is the compressor map used for a wide range of fan radii, which leads to extrapolation of the curves.

DOI: 10.13009/EUCASS2022-6105

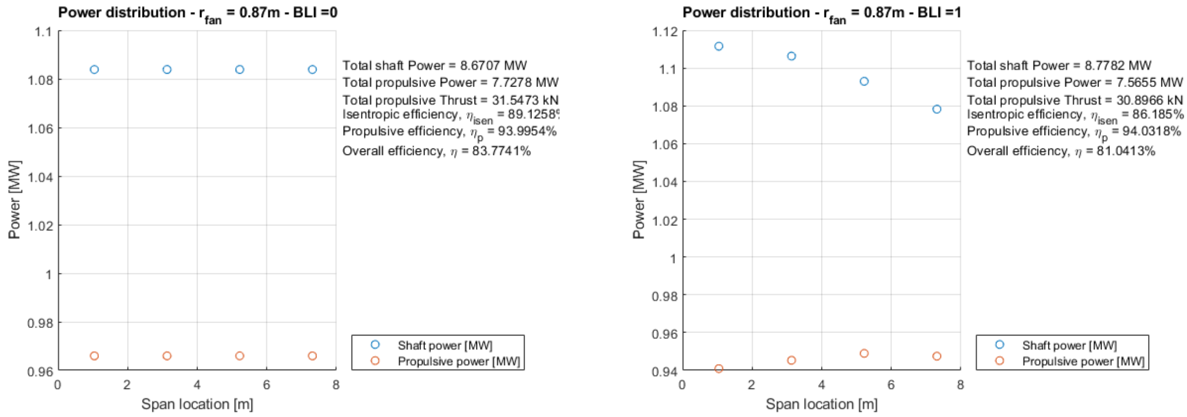

(a) DEP performance - 8 thrusters (BLI is off)

(b) DEP performance - 8 thrusters (BLI is on)

Figure 10: DEP performance comparison between BLI off and BLI on. Fan radius is $0.87m$.

Regarding the latter, the behaviour of the propulsor in terms of isentropic efficiency and fan pressure ratio was assumed behaviour by the author.

It is shown that the Power Savings Coefficient is in the order of $2-3\%$ depending on the C_L value. The power savings coefficient is smaller with higher C_L as the required propulsive power increases with increasing C_L, while the absolute power saving is about the same. The added benefit of adding propulsors to the array decreases. Moreover, it is shown that the array is bound to geometrical constraints as it has to fit on the 'square like' trailing edge of the Blended Wing Body. Therefore, it was determined that an array of 8 propulsors is the maximum attainable to fit on the aircraft. Regarding the shaft power consumption of the aircraft, it was shown that the optimum operating point in terms of isentropic efficiency was at around a fan radius of about $0.9m$ while the minimum propulsive power consumption was at about a fan radius of about $0.5m$. Therefore, an 'optimum' fan configuration is dependent on the figure of merit (propulsive power versus shaft power).

6. Acknowledgments

The reported work has been performed within the framework of the IMOTHEP project. The authors acknowledge the valuable discussions and contributions of IMOTHEP partners to this work as well as the funding received from the European Union Horizon 2020 programme under grant agreement No. 875006.

References

[1] Aurélien Arntz and Olivier Atinault. Exergy-based performance assessment of a blended wing–body with boundary-layer ingestion. *AIAA journal*, 53(12):3766–3776, 2015.

[2] Thomas Bontemps. Imothep report d2.3: Optimized design of thruster/ogv/channel under bli interaction, 2022.

[3] Nils Budziszewski and Jens Friedrichs. Modelling of a boundary layer ingesting propulsor. *Energies*, 11(4):708, 2018.

[4] Mark Drela. Power balance in aerodynamic flows. *AIAA journal*, 47(7):1761–1771, 2009.

[5] J. Gauvrit and Q. Bennehard. Description of nacor-derived smile bwb geometry and characteristics, 2022.

[6] Ron Hendrickson. *FRICTION*. Virginia Tech Aerodynamics and Design Software Collection, 2015.

[7] Jin Kim, Kevin Kwon, Sayan Roy, Elena Garcia, and Dimitri N Mavris. Megawatt-class turboelectric distributed propulsion, power, and thermal systems for aircraft. In *2018 AIAA Aerospace Sciences Meeting*, page 2024, 2018.

[8] Robert Larkens. A coupled propulsion and thermal management system for hybrid electric aircraft design: A case study. 2020.

[9] Angélique Pascale Plas. *Performance of a boundary layer ingesting propulsion system*. PhD thesis, Massachusetts Institute of Technology, 2006.

DOI: 10.13009/EUCASS2022-6105

[10] Sho Sato et al. *The power balance method for aerodynamic performance assessment*. PhD thesis, Massachusetts Institute of Technology, 2012.

[11] Alessandro Sgueglia. *Methodology for sizing and optimising a Blended Wing-Body with distributed electric ducted fans*. PhD thesis, 12 2019.

[12] J. van de Vooren and A.J. van der Wees. Drag prediction for transonic transport aircraft using a full-potential method, 1993.

[13] A van der Wees, J Van Muijden, and J Van der Vooren. A fast robust viscous-inviscid interaction solver for transonic flow about wing/body configurations on the basis of full potential theory. In *23rd Fluid Dynamics, Plasmadynamics, and Lasers Conference*, page 3026, 1993.

[14] J van Muijden, A.J. van der Wees, and J van der Vooren. Flow analysis and drag prediction for transonic transport wing/body configurations using a viscous-inviscid interaction type method, 1994.